Forming mechanism of the bipolar resistance switching in double-layer memristive nanodevices

2012 Nanotechnology 23 315202

(http://iopscience.iop.org/0957-4484/23/31/315202)

Nanotechnology **23** (2012) 315202 (9pp) doi:10.1088/0957-4484/23/31/315202

Forming mechanism of the bipolar resistance switching in double-layer memristive nanodevices

S B Lee[1,2], H K Yoo[1,2], K Kim[2], J S Lee[2,3], Y S Kim[1,2], S Sinn[1,2], D Lee[4], B S Kang[5], B Kahng[2] and T W Noh[1,2]

[1] IBS-Research Center for Functional Interfaces, Seoul National University, Seoul 151-747, Republic of Korea
[2] Department of Physics and Astronomy, Seoul National University, Seoul 151-747, Republic of Korea
[3] School of Physics, Korea Institute for Advanced Study, Seoul 130-722, Republic of Korea
[4] Semiconductor Device Laboratory, Samsung Advanced Institute of Technology, Samsung Electronics, Yongin, Gyeonggi-do 446-712, Republic of Korea
[5] Department of Applied Physics, Hanyang University, Ansan, Gyeonggi-do 426-791, Republic of Korea

E-mail: twnoh@snu.ac.kr

Received 9 April 2012, in final form 18 June 2012
Published 17 July 2012
Online at stacks.iop.org/Nano/23/315202

Abstract
To initiate resistance switching phenomena, it is usually necessary to apply a strong electric field to a sample. This forming process poses very serious obstacles in real nanodevice applications. In unipolar resistance switching (URS), it is well known that the forming originates from soft dielectric breakdown. However, the forming in bipolar resistance switching (BRS) is poorly understood. In this study, we investigated the forming processes in $Pt/Ta_2O_5/TaO_x/Pt$ and $Pt/TaO_x/Pt$ nanodevices, which showed BRS and URS, respectively. By comparing the double- and single-layer systems, we were able to observe differences in the BRS and URS forming processes. Using computer simulations based on an 'interface-modified random circuit breaker network model', we could explain most of our experimental observations. This success suggests that the BRS forming in our $Pt/Ta_2O_5/TaO_x/Pt$ double-layer system can occur via two processes, i.e., polarity-dependent resistance switching in the Ta_2O_5 layer and soft dielectric breakdown in the TaO_x layer. This forming mechanism can be used to improve the performance of BRS devices. For example, we could improve the endurance properties of $Pt/Ta_2O_5/TaO_x/Pt$ cells by using a small forming voltage.

(Some figures may appear in colour only in the online journal)

1. Introduction

Resistance switching (RS) phenomena refer to alternating changes between two metastable resistance states driven by an external voltage [1–3]. Since the early 1960s, RS phenomena have been observed in numerous material systems, including binary oxides, complex perovskite oxides, sulfides, semiconductors, and organics [1]. In the 1960s, Hiatt and Hickmott had already mentioned the possible use of the RS phenomena in memories [4]. Such a possibility became realized later in nonvolatile memory devices, called 'resistance random access memory (RRAM)' [5–23]. Recently, Strukov *et al* noted that RS devices, such as $Pt/TiO_2/Pt$ cells, could be considered 'memristors', which had been regarded as the missing fourth fundamental circuit element [9–14]. Some researchers proposed using RS devices as adaptive electronic components, because their learning behaviours resemble those of the human brain [23–25]. Consequently, there has been a flurry of investigation into RS phenomena because of the inherent scientific interest and the potential for practical applications [1–26].

Forming is required to initiate the RS phenomena for most samples [3–23]. It should be noted that most as-grown cells do not show the RS phenomenon. To observe the RS phenomenon, we must apply a large voltage (or a large current) to a pristine cell. This process generates conducting channels throughout the cell, which provide the current pathway for the following RS operations. Although forming is essential for most RS phenomena, there has been little investigation into it because many highly uniform samples are required, as described in section 3.1. Moreover, forming usually requires an operating voltage that is significantly larger than those for RS between the metastable states [3–23]. Because it is difficult to control and frequently damages the cells [11, 22], the forming process is considered a large obstacle to the realization of RRAM applications.

RS phenomena can be separated into two types based on their electric polarity dependence [1–25]. In unipolar RS (URS), the corresponding current–voltage (I–V) curves are quite symmetric and both resistance changes between insulating and conducting states can occur in any polarity. So, only one voltage polarity is needed for its operation. In bipolar RS (BRS), the curves are quite asymmetric and a change from insulating to conducting state can occur in one polarity and the reverse change can occur in the opposite polarity. So, both polarities are required.

During the URS forming process, soft dielectric breakdown can occur via a percolation process across the cell [27–29]. We suggested that the conducting channels formed by the soft dielectric breakdown will have a fractal structure, which could explain the voltage-/current-driven RS [20], the wide distribution of set and reset voltages [20, 30–32], multilevel switching [33], the scaling behaviours of the reset voltages and currents [30–32], and the large $1/f$ noise [34]. Due to the nature of the percolation process, the required forming voltage V_F is large and always accompanied with very large fluctuations [30–32]. These characteristics of V_F pose drawbacks in the application of URS in RRAM. By comparison, BRS forming process usually do not reveal such drawbacks related to V_F. However, BRS forming still possesses some undesirable characteristics, including effects on device reliabilities [11, 35, 36], and its mechanism is not yet fully understood. Therefore, for successful bipolar RRAM operations, the basic mechanism of BRS forming must be fully understood so that successful methods to control it can be developed.

Here, we report our systematic studies on BRS forming in Pt/Ta_2O_5/TaO_x/Pt cells. Note that Pt/TaO_x/Pt cells show URS [37], in which the forming is known to originate from the soft dielectric breakdown [27–29]. We selected Pt/Ta_2O_5/TaO_x/Pt cells as a model system because BRS can be easily obtained by inserting a thin insulating Ta_2O_5 layer [37]. Comparative studies with Pt/Ta_2O_5/TaO_x/Pt and Pt/TaO_x/Pt cells provide an opportunity to understand BRS forming based on the comparatively well-established forming mechanism of URS. In addition, Pt/Ta_2O_5/TaO_x/Pt cells were selected because they have significant potential in real applications [15]. Recently, Lee *et al* demonstrated that Pt/Ta_2O_5/TaO_x/Pt nanodevices possess excellent BRS properties, including fast switching, high scalability, long retention, and high endurance [15]. Therefore, our findings on the BRS forming of Pt/Ta_2O_5/TaO_x/Pt cells can advance potential applications as well as providing deeper insight into its physical mechanisms.

2. Experimental method

We fabricated Pt/Ta_2O_5/TaO_x/Pt and Pt/TaO_x/Pt cells with the cell geometries shown in figures 1(a) and (d), respectively. We first deposited 50 nm thick bottom Pt electrode layers on Ti (10 nm)/SiO_2 (500 nm)/Si substrates by RF magnetron sputtering. We then grew 40 nm thick TaO_x layers on the Pt layers using reactive RF magnetron sputtering. The TaO_x layers were grown at 3% oxygen partial pressure in an Ar + O_2 gas flow of 5 mTorr total pressure and at a substrate temperature of 400 °C. To insert the Ta_2O_5 layer, plasma annealing was carried out at 500 °C in a chamber with argon and 10% oxygen plasma. Analysis showed that with 5 min of oxygen plasma exposure, the approximately 10 nm thick top TaO_x layer was transformed into a stoichiometric Ta_2O_5 layer. The next step was to deposit a top Pt electrode layer on the Ta_2O_5/TaO_x/Pt and TaO_x/Pt cells by RF magnetron sputtering. Using standard photolithography and lift-off methods, we finally made the Pt/Ta_2O_5/TaO_x/Pt and Pt/TaO_x/Pt cells. To fabricate the Pt/TaO_x/Pt reference cells, we used the same procedure but without the plasma annealing process.

We analysed the Pt/Ta_2O_5/TaO_x/Pt and Pt/TaO_x/Pt cells using cross-sectional transmission electron microscopy (TEM) and x-ray photoelectron spectroscopy (XPS) depth profiles. For the XPS depth profile, we used monochromatic Al Kα ($h\nu = 1486.6$ eV) x-rays with a beam power of 27.7 W and a beam size of 20 μm. We monitored the depth profiles of the Pt/Ta_2O_5/TaO_x/Pt and Pt/TaO_x/Pt cells by varying the Ar^+-ion sputtering time.

We measured the I–V characteristics at room temperature using an Agilent 4155C semiconductor-parameter analyser. During all the electrical measurements, we grounded the bottom Pt electrodes and applied the voltage to the top Pt electrodes. We swept the voltage for 4 s. We applied a pulse signal to the cells using a Yokogawa FG200 synthesized function generator. To confirm forming, we monitored the output current simultaneously throughout the cell using a Yokogawa DL7100 digital oscilloscope. To prevent deformation of the signal shape by impedance mismatching, we let the pulse voltage pass through an nF HSA4101 high-speed bipolar amplifier.

3. Comparative experimental studies of BRS and URS forming

3.1. Cell characterization

Figure 1(a) schematically shows the geometry of the Pt/TaO_x/Pt cells used in this study. Figure 1(b) displays the cross-sectional TEM image of a Pt/TaO_x/Pt cell. Figure 1(c) shows XPS depth profile analysis of the Pt/TaO_x/Pt cells. The relative atomic concentration depth distributions of Pt, Ta, and

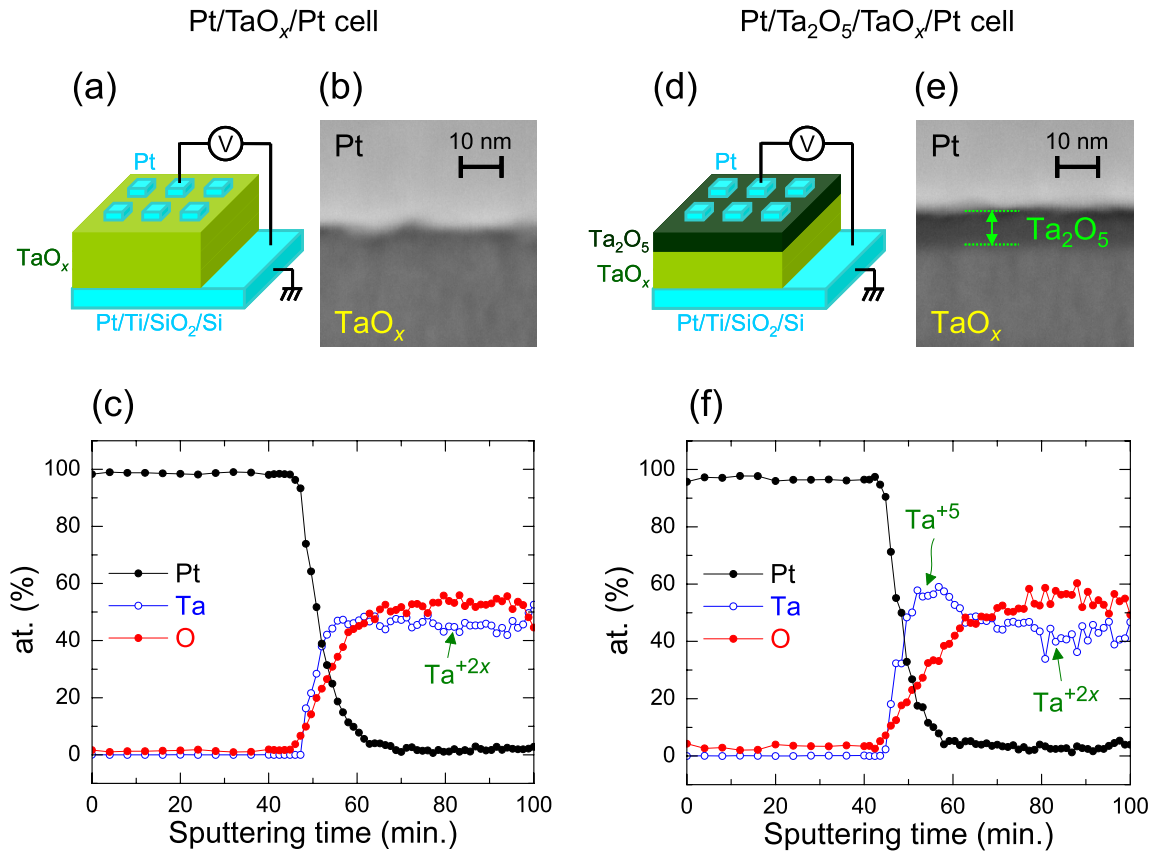

Figure 1. (a) The cell geometry of a Pt/TaO_x/Pt cell. We confirmed the absence of a Ta_2O_5 layer between the Pt electrode and the TaO_x layer using (b) cross-sectional TEM and (c) XPS depth profile analysis. (d) Cell geometry of a Pt/Ta_2O_5/TaO_x/Pt cell. We similarly confirmed that a stoichiometric Ta_2O_5 layer was effectively formed on the TaO_x layer using (e) cross-sectional TEM and (f) XPS depth profile analysis.

O, which are evaluated from the XPS peaks of Pt 4f, Ta 4f, and O 1s, are shown as a function of Ar^+-ion sputtering time. This figure shows that a rather clean interface formed between the Pt and TaO_x layers in the Pt/TaO_x/Pt cells.

Figures 1(d) and (e) show the geometry and cross-sectional TEM image of a Pt/Ta_2O_5/TaO_x/Pt cell, respectively. The TEM image shows that an approximately 10 nm thick Ta_2O_5 layer formed on top of the TaO_x layer. As shown in the XPS depth profile (figure 1(f)), a peak corresponding to Ta^{+5} was significantly enhanced between the Pt and TaO_x layers, which supports the formation of the Ta_2O_5 layer.

It should be noted that our Pt/Ta_2O_5/TaO_x/Pt cells have very high uniformity in their electrical properties. It is difficult to investigate forming because it is an irreversible process. That is, after we apply V_F to any cell, conducting channels form. These channels will be broken and reconnected by the following operations, but cannot be removed completely [20–22]. Therefore, to experimentally investigate the basic mechanism of forming, each pristine cell can only be used once in forming studies. This means that many cells with very similar RS characteristics are required to reduce the large fluctuations in the statistical averages and thereby obtain meaningful data. To test the uniformity of our cells, we randomly chose about 100 cells that had been fabricated in the same batch and measured their *I*–*V* curves. At −3 V, their current values remained nearly the same at −2.5 nA with a standard deviation of 4%. This excellent uniformity allowed us to study the intriguing behaviour of BRS forming in Pt/Ta_2O_5/TaO_x/Pt cells.

3.2. URS forming characteristics in Pt/TaO_x/Pt cells

The *I*–*V* curves for the Pt/TaO_x/Pt cells exhibited URS. The pristine cells were in the insulating state. As indicated by the black line in figure 2(a), forming could be driven by applying a negative V_F of around −5 V. Just after this forming, the Pt/TaO_x/Pt cell was in a conducting (on-) state. When we applied a negative voltage again, it reset into an insulating (off-) state, a process known as 'reset'. By applying a higher negative voltage, we could change the cell back into the on-state, a process known as 'set'. To avoid permanent Joule heating damage of the cell, we needed to externally limit the compliance current flow, I_{comp}, during both the forming and the set processes. In this experiment, we used an I_{comp} of −30 mA. As shown in figure 2(b), the *I*–*V* curves are quite symmetric about the change in voltage polarity, indicating that the RS in the Pt/TaO_x/Pt cell is unipolar.

It should be noted that just after URS forming, the Pt/TaO_x/Pt cells enter the on-state irrespective of the V_F polarities. Figure 2(a) shows that, as indicated by the star, applying a negative V_F causes the cell to enter the on-state; Figure 2(b) shows that, as indicated by the diamond, the

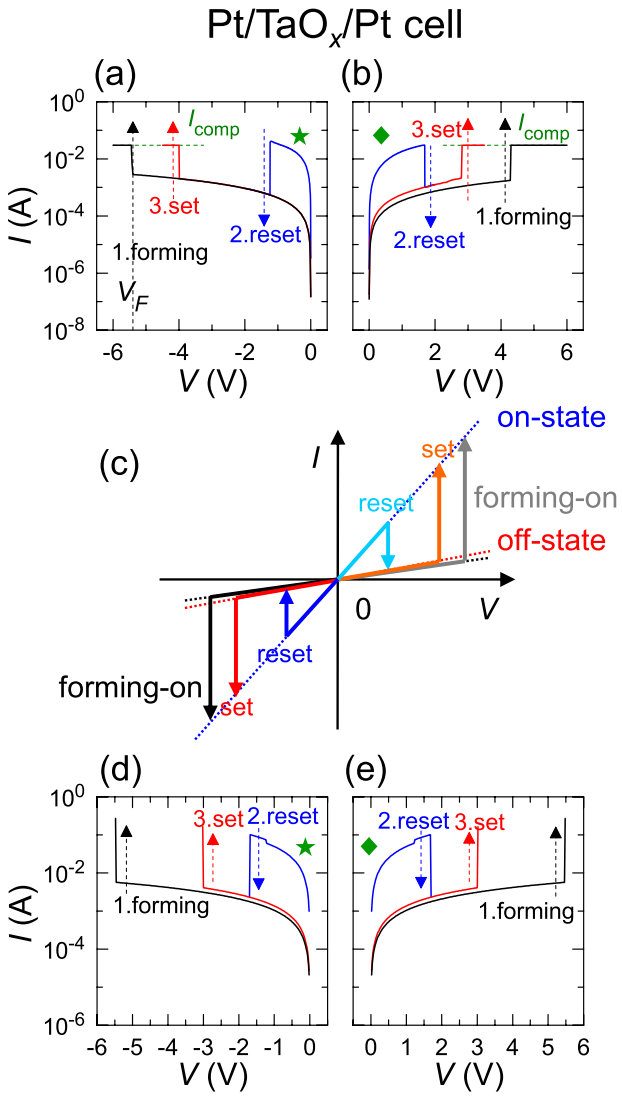

Figure 2. *I–V* curves of Pt/TaO_x/Pt cells after URS forming with (a) negative and (b) positive polarities. As indicated by the star and diamond symbols, the cells always enter the on-state after URS forming. (c) Schematic diagram of the *I–V* curves after URS forming. The simulation results after URS forming under (d) negative and (e) positive polarities agree quite well with the experimental results.

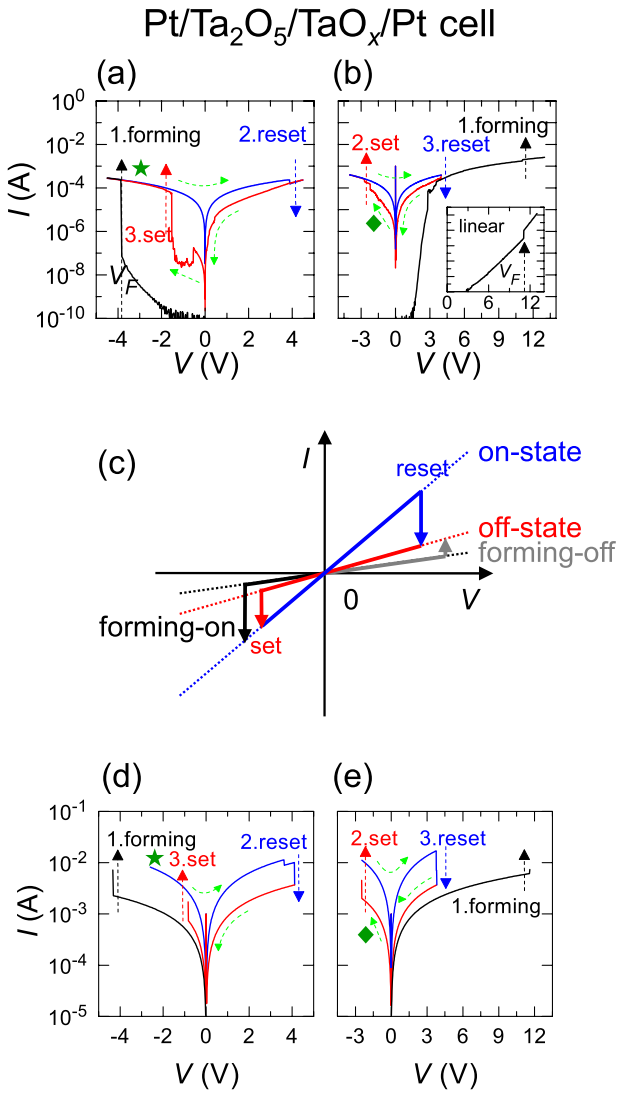

Figure 3. *I–V* curves of Pt/Ta_2O_5/TaO_x/Pt cells after BRS forming under (a) negative and (b) positive polarities. The inset of figure 3(b) shows *I–V* curves of BRS forming under positive polarity in a linear scale. As indicated by the star (diamond) symbols, the cells enter the on (off)-state after BRS forming under negative (positive) polarity. (c) Schematic diagram of the *I–V* curves after BRS forming. The simulation results after BRS forming under (d) negative and (e) positive polarities agree quite well with the experimental results.

same is true when positive V_F is applied. These results are schematically depicted in figure 2(c). Similar observations have also been made in many other URS systems [20, 21].

3.3. BRS forming characteristics in Pt/Ta_2O_5/TaO_x/Pt cells

The *I–V* curves for the Pt/Ta_2O_5/TaO_x/Pt cells exhibited BRS. As indicated by the black line in figure 3(a), the current flow increased suddenly when we applied a negative V_F of around −4 V. After this forming, the Pt/Ta_2O_5/TaO_x/Pt cell was in the on-state. The reset process occurred when we applied a positive voltage of about +4 V. The set process then occurred when we applied a negative voltage of around −2 V. During these BRS forming and set processes, the self-limited current flow naturally occurred at a value of about −0.3 mA. It should be noted that the Pt/Ta_2O_5/TaO_x/Pt cells require both voltage polarities to change reversibly between on-states and off-states, indicating that their RS is bipolar.

In contrast to URS, the Pt/Ta_2O_5/TaO_x/Pt cells enter different resistance states just after BRS forming, depending on the V_F polarities. Figure 3(a) shows that by applying a negative V_F, the BRS cell enters the on-state, again indicated by a star symbol. As shown in figure 3(b), the cell enters the off-state when a positive V_F is applied, as indicated by the diamond symbol. Note that the magnitude of positive V_F is much larger than that of negative V_F. This asymmetry in the BRS forming is closely related to the Ta_2O_5 layer, which breaks the symmetric geometry of the Pt/TaO_x/Pt cell, as shown schematically in figure 3(c). A similar phenomenon was reported for BRS in TiO_2 systems by Yang *et al* [10, 11].

3.4. Other differences between BRS and URS forming

During the BRS forming process, the current change for negative V_F is considerably more abrupt than that for positive V_F. As shown in figure 3(a), the current jumps abruptly from 70 nA to 200 μA (i.e., by four orders of magnitude) when a negative V_F is applied. On the other hand, as shown in figure 3(b), the current increases much less abruptly from 1.5 mA to 2.2 mA when a positive V_F is applied. Conversely, during the URS forming process, as shown in figures 2(a) and (b), the current changes at V_F are nearly the same for both polarities.

When a negative V_F is applied, the magnitude of V_F (i.e., $|V_F|$) of BRS is always smaller than that of URS, as shown in figures 2(a) and 3(a). To investigate this interesting behaviour more systematically, we performed the forming operations with 50 cells for each RS by applying negative V_F. Figure 4(a) displays the cumulative probability $W(|V_F|)$ curves for both BRS and URS. As indicated by the closed red circles, most $|V_F|$ values for BRS are between 3.7 and 4.5 V. On the other hand, as indicated by the open blue circles, most $|V_F|$ values for URS are between 5.1 and 5.9 V. Although the $|V_F|$ values of BRS are significantly smaller than those of URS, the size of the fluctuation (or standard deviation) is nearly the same. On the contrary, when a positive V_F is applied, the $|V_F|$ of BRS is always larger than that of URS, as shown in figures 2(b) and 3(b). (However, in this case, the current change at V_F is not abrupt, as shown in the inset of figure 3(b), so we did not perform the above statistical studies in figure 4(a).)

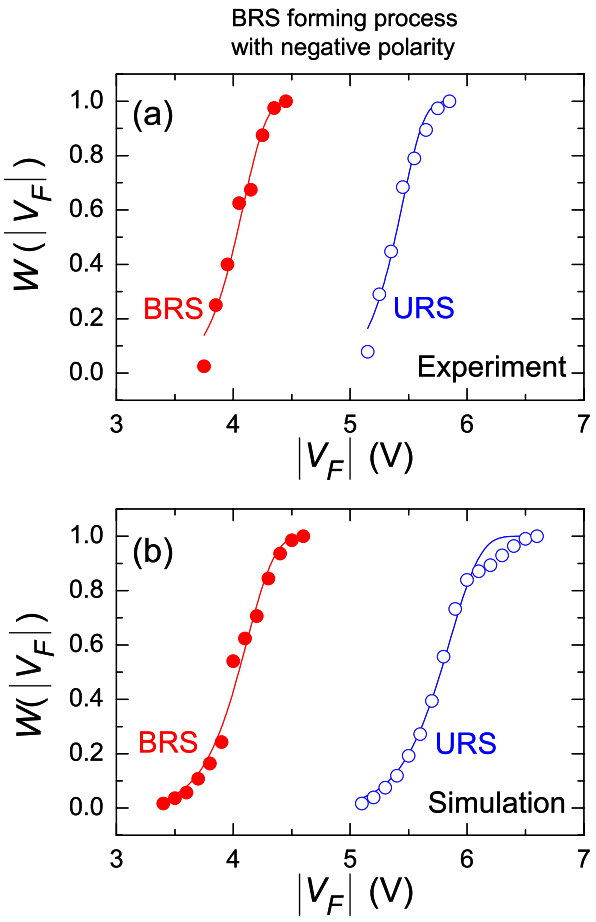

Figure 4. Cumulative probability of the $|V_F|$ distribution for BRS forming with negative polarity obtained by (a) experiments and (b) computer simulations. The closed red circles and blue open circles represent the $|V_F|$ distributions for BRS and URS, respectively.

4. Computer simulation studies of BRS forming

A few years ago, we introduced a new type of percolation model, the random circuit breaker (RCB) network model, to explain most of the experimental characteristics of URS [20]. In this statistical physics model, we approximated the RS medium as an electrical network composed of circuit breakers with bistable states. Simulations based on the RCB network model demonstrated that URS can be explained in terms of collective connectivity changes of conducting channels, i.e., circuit breakers in the on-state. In particular, URS forming can be viewed as the generation of a percolating conducting channel under an external voltage, which corresponds to a soft dielectric breakdown in nature.

It should be noted that the only difference between the geometries of Pt/Ta_2O_5/TaO_x/Pt and Pt/TaO_x/Pt cells is the existence of the highly insulating Ta_2O_5 layer near the top electrode. Therefore, we have to explain how the insertion of a Ta_2O_5 layer can convert the URS of Pt/TaO_x/Pt cells into BRS. In addition, we have to explain all the experimental observations that were made during BRS forming, as reported in section 3.

4.1. The interface-modified random circuit breaker network model

To understand BRS forming in Pt/Ta_2O_5/TaO_x/Pt cells, we used simulations based on the interface-modified RCB network model [37, 38]. Note that this modified percolation model provides a unified scheme that can explain BRS as well as URS [37, 38]. As shown schematically in figure 5, this model divides the switching medium into two regions, each of which is represented by a network composed of circuit breakers with different bistable resistance states. The green and grey circuit breakers in figure 5 represent the Ta_2O_5 and TaO_x layers, respectively.

For each kind of circuit breaker, we should provide proper switching rules between the corresponding bistable resistance states. Because the TaO_x layer showed URS, we presented switching rules between its bistable states with low resistance r_l^{bulk} (the red circuit breakers) and high resistance r_h^{bulk} (the grey circuit breakers). For URS, both selection rules are assumed to be independent of the voltage polarities, as displayed at the bottom of figure 5. For the Ta_2O_5 layer, we assumed that the interfacial layer has other bistable states with low resistance r_l^{int} ($>r_l^{bulk}$, the black circuit breakers) and high resistance r_h^{int} ($>r_h^{bulk}$, the green circuit breakers). To explain the BRS behaviour, we assumed that the switching rules between r_l^{int} and r_h^{int} depend on the voltage polarities, as displayed at the top of figure 5. The polarity dependence

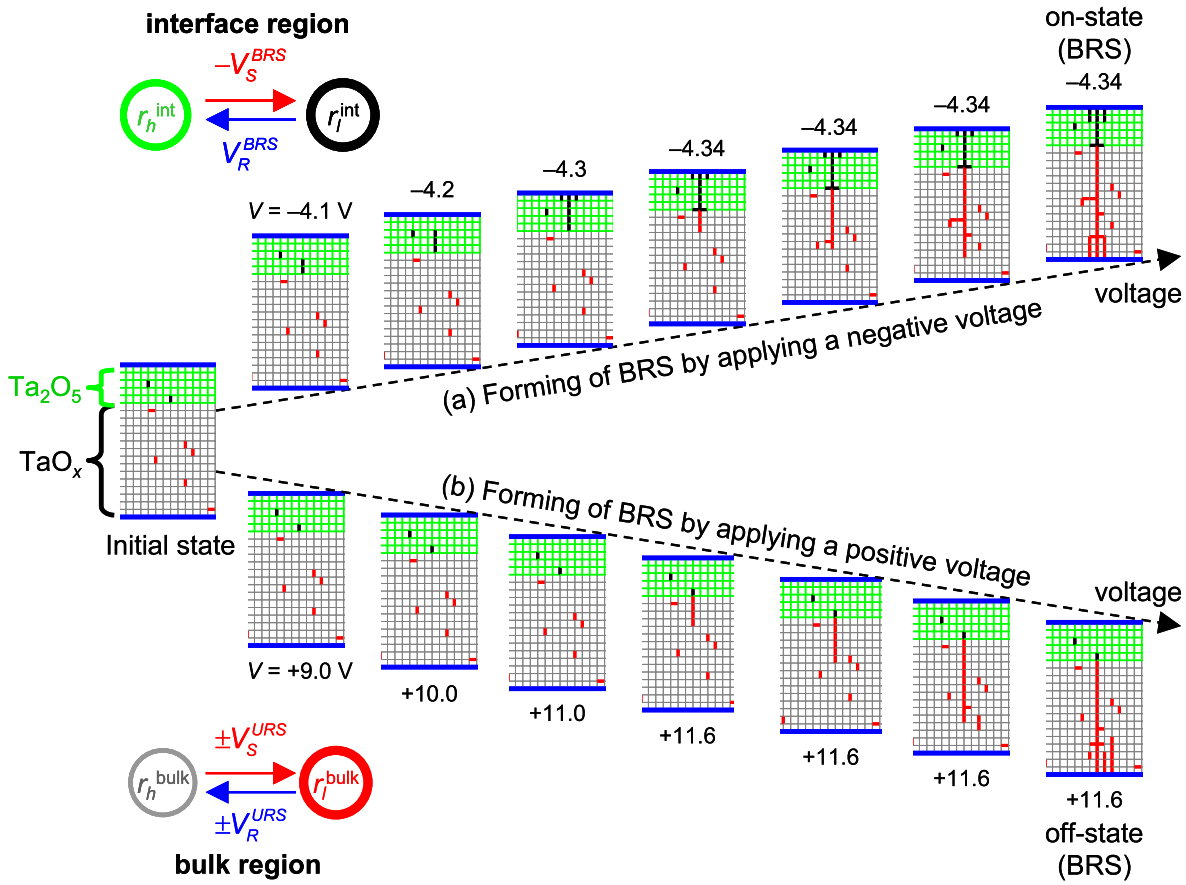

Figure 5. Snapshots of the conducting channels generated by computer simulations based on the interface-modified RCB network model. The left diagram is the initial configuration of circuit breakers. (a) After BRS forming under negative polarity, the cell should enter the on-state because the circuit breakers of r_l^{int} are locally connected inside the interfacial region. (b) After BRS forming under positive polarity, the cell should enter the off-state because all circuit breakers in the interfacial region remain insulating.

of the switching rules between r_h^{int} and r_l^{int} should have microscopic origins, such as movement of oxygen vacancies in the interface region [5–7, 9–15].

To describe forming and the following operational processes of BRS in Pt/Ta_2O_5/TaO_x/Pt cells, we performed computer simulations in a two-dimensional bond percolation network of 19 × 40 circuit breakers. Even though the samples used in our experiments were three-dimensional objects, we think that two-dimensional simulation is sufficient due to the vertical direction of the electric field to the electrode. In figure 5, the top five rows represent the interfacial region and the following 14 rows represent the bulk region. To represent the inhomogeneity of a pristine cell, we assumed that small randomly chosen portions of the circuit breakers are initially in the low-resistance states in the interfacial and bulk regions. To describe BRS forming in the single-layer system, i.e., the Pt/TaO_x/Pt cells, we also performed computer simulations without the interfacial region.

The details of the switching rules and simulation conditions are as follows. We used resistance values of r_h^{int} = 10 000 Ω, r_l^{int} = 200 Ω, r_h^{bulk} = 2000 Ω, and r_l^{bulk} = 1 Ω. We imposed the constraint that the 19 × 40 lattice be linked with a periodic boundary condition in the row. We applied an external voltage V_{ext} along the vertical direction. To describe the initial inhomogeneity inside the cell, we assumed that about 2% of the circuit breakers were in the r_l^{int} and r_l^{bulk} states in the interfacial and bulk regions, respectively. With this initial lattice, we increased V_{ext} from zero. At each voltage step, we calculated all the voltages across each bond Δv by solving the Laplace equation with the boundary condition for fixed V_{ext}. In this simulation, we used the successive over-relaxation method to obtain the set of Δv [39].

With the calculated set of Δv for a given configuration, we checked whether resistance switching could occur in any circuit breakers. In the interfacial region, $r_h^{int} \rightarrow r_l^{int}$ when $|\Delta v| > V_S^{BRS}$ and $V_{ext} < 0$, and $r_l^{int} \rightarrow r_h^{int}$ when $|\Delta v| > V_R^{BRS}$ and $V_{ext} > 0$. We used $V_S^{BRS} = 0.75$ V and $V_R^{BRS} = 0.75$ V in the simulations. Conversely, in the bulk region, $r_h^{bulk} \rightarrow r_l^{bulk}$ when $|\Delta v| > V_S^{URS}$, and $r_l^{bulk} \rightarrow r_h^{bulk}$ when $|\Delta v| > V_R^{URS}$. We used $V_S^{URS} = 0.45$ V and $V_R^{URS} = 0.10$ V ($V_S^{URS} > V_R^{URS}$). Using these switching rules, we checked whether switching could occur for each circuit breaker. When switching did not occur in any circuit breaker, we increased V_{ext} and repeated the calculations. However, when switching occurred for at least one circuit breaker, we recalculated all Δv across each bond for the fixed V_{ext}. We repeated this time evolution process until an equilibrium state was reached.

4.2. Simulation results for both URS and BRS

Our computer simulations, based on the interface-modified RCB network model, can explain most of the experimental observations of URS and BRS. (1) For the single-layer system, they predict the URS phenomena, as indicated by figures 2(d) and (e). The predicted *I*–*V* curves are symmetric about the polarity change. (2) For the double-layer system, they predict that BRS can occur. As shown in figures 3(d) and (e), the predicted *I*–*V* curves are asymmetric about the polarity change. Comparison of the simulation results with the corresponding experimental data demonstrates how well our simulations can describe most of the details of our experimental results.

In addition, our simulations can explain all the experimental observations of both URS and BRS forming. (3) After URS forming, the cell enters the on-state for both polarities, as indicated by the star and diamond symbols in figures 2(d) and (e). Conversely, after BRS forming, the cell enters the on (off)-state when negative (positive) V_F is applied, as indicated by the star (diamond) symbols in figures 3(d) and (e). (4) For BRS forming, the current change at negative V_F is much more abrupt than that at positive V_F, as shown in figures 3(d) and (e). (5) Comparisons between the V_F values show that the BRS $|V_F|$ is smaller than that of URS with negative V_F, and vice versa. We also performed many simulations and calculated the $W(|V_F|)$ curves for negative V_F. As shown in figure 4(b), the $|V_F|$ of BRS is smaller than that of URS with negative V_F.

4.3. Basic mechanisms of BRS forming

One advantage of the computer simulations based on the interface-modified RCB network models is that we can look at a snapshot of the circuit breaker configurations for a desired state and visualize what happens during each process. To understand the basic mechanisms of BRS forming, we looked into the circuit breaker configuration while we swept the applied voltage. Figure 5 shows the configuration changes while we increased V with either negative or positive polarities in a sweep mode. Out of the 19×40 square lattice, we only show the region where a nearly percolating channel with r_l^{int} and r_l^{bulk} formed. The left snapshot in figure 5 shows the initial configuration. In each series, the first three diagrams show the configurations when $|V| < |V_F|$, and the following diagrams show the time evolution of the configuration at $V = V_F$.

The upper series of configurations in figure 5 shows what happens under negative polarity. Initially, a conducting channel starts to form at the interfacial region. Microscopically, such a channel formation might come from either an oxygen vacancy migration [5–15] or charge trap centres [17–19]. However, in our model, we were only concerned with the connectivity changes in the conducting circuit breakers, so we ignored its microscopic origin. When the conducting channel becomes percolating throughout the interfacial region, soft dielectric breakdown occurs suddenly in the bulk region. The external voltage at this moment corresponds to V_F. After forming, it will enter the on-state, in agreement with the experimental observation in figure 3(a).

Under negative polarity, the BRS $|V_F|$ values are smaller than those of URS. With a different initial configuration, the predicted V_F value can be varied. By choosing the initial configuration randomly, we calculated $W(|V_F|)$ for BRS. The closed red circles in figure 4(b) show $W(|V_F|)$ for BRS forming. We also performed the simulations without the interfacial region, i.e., for URS in the single-layer system. The blue open circles in figure 4(b) show $W(|V_F|)$ for URS forming. In agreement with the experimental result in figure 4(a), the $|V_F|$ of BRS can be smaller. The reason why $|V_F|$ can be smaller for BRS is that the percolating conducting channel in the interfacial region plays the role of a 'lightning rod' for the soft dielectric breakdown in the bulk region, so it becomes easier for BRS to experience soft dielectric breakdown. Furthermore, the associated current change at negative V_F should be quite abrupt.

The lower series of configurations in figure 5 shows what happens under positive polarity. Initially, there are no changes in the conducting channels in either the interfacial or the bulk regions below V_F. When V reaches V_F, soft dielectric breakdown occurs in the bulk region, but a conducting channel percolates through the bulk region only. After forming, it will enter the off-state, in agreement with the experimental observation depicted in figure 3(b). It should be noted that most of the external voltage should be applied to the circuit breakers in the interfacial region due to their higher resistance values. (However, these circuit breakers do not change their resistance states due to the polarity-dependent switching rules.) Thus, $|V_F|$ under positive bias should be much larger than those under negative bias. Furthermore, the current flow at V_F should be limited by the high resistance value of the interfacial region, so the associated current change at positive V_F cannot be as abrupt.

Our simulations, based on the interface-modified RCB network model, can explain all our experimental observations of BRS forming described in section 2. Therefore, the basic mechanism of BRS forming in our Pt/Ta_2O_5/TaO_x/Pt double-layer system can be understood simply in terms of polarity-dependent RS in the Ta_2O_5 layer and soft dielectric breakdown in the TaO_x layer. The soft dielectric breakdown can explain why localized conducting channels have been observed in numerous earlier studies in BRS [5–7, 14]. In addition, our simulations provide an effective way to study BRS behaviour at a quantitative level.

5. The importance of forming in enhancing BRS endurance properties

The endurance of RRAM represents how repetitively resistance can be switched between the on- and off-states, so it is a very important reliability issue for RRAM [15]. By controlling the applied voltage during the forming process, we found that we could improve the endurance of BRS in Pt/Ta_2O_5/TaO_x/Pt cells significantly. To examine the endurance, we drove the BRS forming by applying a pulse signal with a forming voltage value of V_f. (Note that we used

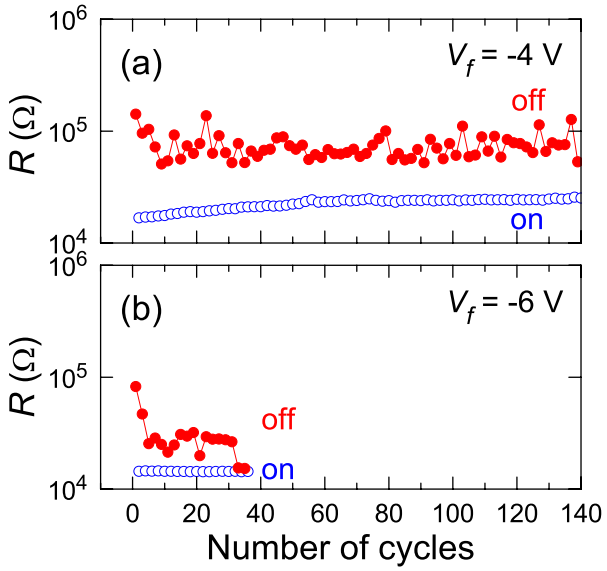

Figure 6. The endurance of BRS in Pt/Ta_2O_5/TaO_x/Pt cells after forming with V_f values of (a) −4 V and (b) −6 V.

a pulse in this experiment, as in the operation of actual RRAM devices.) As described in section 3.3, the compliance current was self-limited in this case. After forming, we performed RS operations between off- and on-states by sweeping voltages of 0 V → +4 V → 0 V (reset) and 0 V → −4 V → 0 V (set), respectively. At each resistance state, we read a resistance value by applying a readout voltage of 0.1 V.

We found that the value of $|V_F|$ can affect the endurance significantly. As shown in figure 6(a), with $V_f = -4$ V, BRS can be repeated many times. However, as shown in figure 6(b), with $V_f = -6$ V, the cell failed to show BRS after only 40 switching cycles, and then the resistance state remained in the on-state. When we increased the sweeping voltage on the failed cell, BRS could be recovered for a while but failed again after a certain number of cycles. In addition, the resistance values of the off-states in figure 6(b) are smaller than those in figure 6(a). At this moment, the origins of such enhanced endurance for the sample formed with lower voltage are not clear. There have been several reports that the endurance property is related to the reversible oxidation and reduction in an interfacial oxide layer by oxygen vacancy or ion movements [40–43]. The excellent agreement between our experimental data and theoretical predictions suggests that collective connectivity changes in the r_l^{int} in our interface-modified RCB network model might mimic the oxygen vacancy or ion movements.

To obtain further insights into what could happen during the forming process with different V_f values, we performed computer simulations using the interface-modified RCB network model and looked at the snapshots of the circuit breaker configurations. The left snapshot in figure 7 displays the initial state configuration. With $V_f = -4.3$ V, the percolating channel first appears in the interfacial region and plays the role of a lightning rod for soft dielectric breakdown in the bulk region. In addition, the percolating channel in the bulk region seems to be singly connected. In the BRS set and reset operations, the percolating channel in the bulk region experiences little change, and all the actions related to set and reset operations occur in the interfacial region [38]. Due to the sharp rod-like geometry of the percolating channel, a very high electric field will be generated in the interfacial region at the end of the bulk percolating channel, which makes the following BRS operations reliable. On the other hand, with $V_f = -5.8$ V, a multitude of thick percolating channels initially appears in the interfacial region. After this, the percolating channels in the bulk region after soft dielectric breakdown appear to be multiply connected. The multiple connection explains why the resistance values of the off-state are smaller than those with lower V_f. Since the relatively dull geometry of the conducting channel could affect the oxygen vacancy movements under external voltage, the RS might be degraded in the later operations. Our simulation

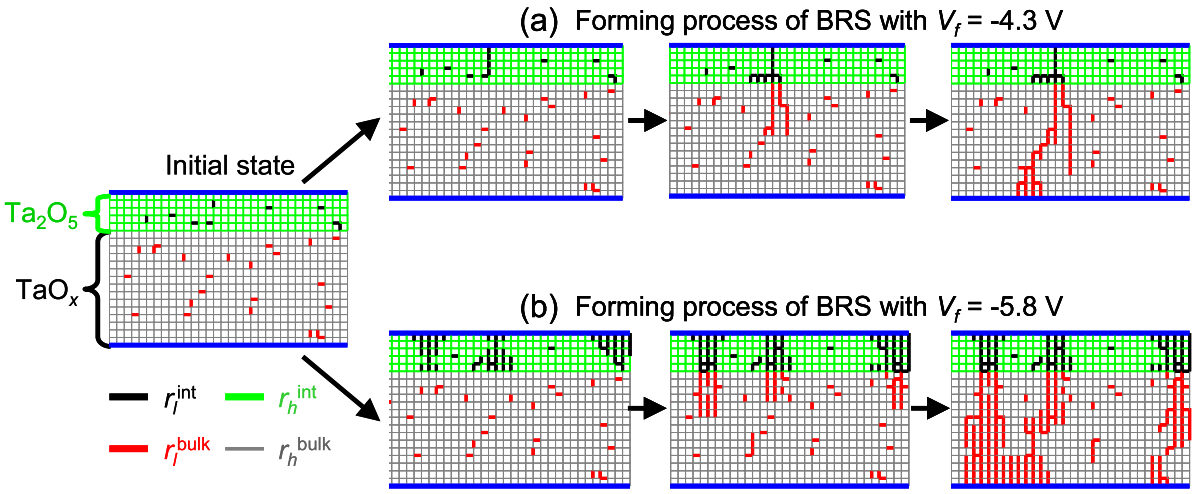

Figure 7. Snapshots of the conducting channels generated by the computer simulations with (a) small V_f (= − 4.3 V) and (b) large V_f (= − 5.8 V).

studies show that further research on the connectivity issue is highly desirable for the understanding of the V_f-dependent endurance. They also indicate that forming voltage control is important for obtaining reliable RRAM operation.

6. Conclusions

We systematically investigated changes in the physical properties of Pt/Ta_2O_5/TaO_x/Pt cells due to BRS forming. To obtain deeper insight, we compared them with URS forming changes in Pt/TaO_x/Pt cells. In this single-layer system, URS forming is known to occur by soft dielectric breakdown. We found that a highly insulating Ta_2O_5 layer can convert URS into BRS and plays important roles in BRS forming. Using the interface-modified RCB network model, we could explain all of the experimental observations of BRS forming in Pt/Ta_2O_5/TaO_x/Pt cells. During the forming of this double-layer system, the percolating channels inside the TaO_x layer occur by polarity-independent soft dielectric breakdown, but those inside the Ta_2O_5 layer occur by polarity-dependent physical processes. Our model explains why the forming is much softer for BRS. We also showed that the endurance properties of BRS can also be enhanced by proper control of the forming.

Acknowledgments

S B Lee and H K Yoo contributed equally to this study. This research was supported by the Institute of Basic Science (IBS) and the National Research Foundation of Korea (NRF) (No. 2012-0005847, (BK) 2010-0015066, (BSK) 2012-0001684, (SBL) NRF-2011-354-C00031, and (JSL) NRF-2011-35B-C00014) grant funded by the Korean government (MEST).

References

[1] Dearnaley G, Stoneham A M and Morgan D V 1970 *Rep. Prog. Phys.* **33** 1129
[2] Meijer G I 2008 *Science* **319** 1625
[3] Ramanathan S 2010 *Thin Film Metal-Oxides: Fundamentals and Applications in Electronics and Energy* (New York: Springer)
[4] Hiatt W R and Hickmott T W 1965 *Appl. Phys. Lett.* **6** 106
[5] Waser R and Aono M 2007 *Nature Mater.* **6** 833
[6] Waser R, Dittmann R, Staikov G and Szot K 2009 *Adv. Mater.* **21** 2632
[7] Muenstermann R, Menke T, Dittmann R and Waser R 2010 *Adv. Mater.* **22** 4819
[8] Sawa A 2008 *Mater. Today* **11** 28
[9] Strukov D B, Snider G S, Stewart D R and Williams R S 2008 *Nature* **453** 80
[10] Yang J J, Pickett M D, Li X, Ohlberg D A A, Stewart D R and Williams R S 2008 *Nature Nanotechnol.* **3** 429
[11] Yang J J, Miao F, Pickett M D, Ohlberg D A A, Stewart D R, Lau C N and Williams R S 2009 *Nanotechnology* **20** 215201
[12] Strukov D B, Borghetti J and Williams R S 2009 *Small* **5** 1058
[13] Borghetti J, Snider G S, Kuekes P J, Yang J J, Stewart D R and Williams R S 2010 *Nature* **464** 873
[14] Miao F, Strachan J P, Yang J J, Zhang M-X, Goldfarb I, Torrezan A C, Eschbach P, Kelley R D, Medeiros-Ribeiro G and Williams R S 2011 *Adv. Mater.* **23** 5633
[15] Lee M-J *et al* 2011 *Nature Mater.* **10** 625
[16] Chang S H *et al* 2011 *Adv. Mater.* **23** 4063
[17] Rozenberg M J, Inoue I H and Sánchez M J 2004 *Phys. Rev. Lett.* **92** 178302
[18] Chen A B K, Kim S G, Wang Y, Tung W-S and Chen I-W 2011 *Nature Nanotechnol.* **6** 237
[19] Choi B J, Chen A B K, Yang X and Chen I-W 2011 *Adv. Mater.* **23** 3847
[20] Chae S C *et al* 2008 *Adv. Mater.* **20** 1154
[21] Lee M-J *et al* 2009 *Nano Lett.* **9** 1476
[22] Kwon D-H *et al* 2010 *Nature Nanotechnol.* **5** 148
[23] Ha S D and Ramanathan S 2011 *J. Appl. Phys.* **110** 071101
[24] Jo S H, Chang T, Ebong I, Bhadviya B B, Mazumder P and Lu W 2010 *Nano Lett.* **10** 1297
[25] Ohno T, Hasegawa T, Tsuruoka T, Terabe K, Gimzewski J K and Aono M 2011 *Nature Mater.* **10** 591
[26] Hino T, Tanaka H, Hasegawa T, Aono M and Ogawa T 2010 *Small* **6** 1745
[27] O'Dwyer J J 1973 *The Theory of Electrical Conduction and Breakdown in Solid Dielectrics* (Oxford: Clarendon)
[28] Inoue I H, Yasuda S, Akinaga H and Takagi H 2008 *Phys. Rev.* B **77** 035105
[29] Lee S B, Yoo H K, Chang S H, Gao L G, Kang B S, Lee M-J, Kim C J and Noh T W 2011 *Appl. Phys. Lett.* **98** 053503
[30] Lee S B, Chae S C, Chang S H, Lee J S, Seo S, Kahng B and Noh T W 2008 *Appl. Phys. Lett.* **93** 212105
[31] Lee J S, Lee S B, Chang S H, Gao L G, Kang B S, Lee M-J, Kim C J, Noh T W and Kahng B 2010 *Phys. Rev. Lett.* **105** 205701
[32] Lee J S and Kahng B 2011 *Phys. Rev.* E **83** 052103
[33] Chae S C, Lee J S, Choi W S, Lee S B, Chang S H, Shin H, Kahng B and Noh T W 2009 *Appl. Phys. Lett.* **95** 093508
[34] Lee S B *et al* 2009 *Appl. Phys. Lett.* **95** 122112
[35] Jeong D S, Schroeder H, Breuer U and Waser R 2008 *J. Appl. Phys.* **104** 123716
[36] Nauenheim C, Kuegeler C, Ruediger A and Waser R 2010 *Appl. Phys. Lett.* **96** 122902
[37] Yoo H K *et al* 2011 *Appl. Phys. Lett.* **98** 183507
[38] Lee S B, Lee J S, Chang S H, Yoo H K, Kang B S, Kahng B, Lee M-J, Kim C J and Noh T W 2011 *Appl. Phys. Lett.* **98** 033502
[39] Conte S D and de Boor C 1980 *Elementary Numerical Analysis: An Algorithmic Approach* (New York: McGraw-Hill)
[40] Lin C Y, Wu C Y, Wu C Y, Tseng T Y and Hu C 2007 *J. Appl. Phys.* **102** 094101
[41] Shen W, Dittmann R, Breuer U and Waser R 2008 *Appl. Phys. Lett.* **93** 222102
[42] Hasan M, Dong R, Choi H J, Lee D S, Seong D J, Pyun M B and Hwang H 2008 *Appl. Phys. Lett.* **92** 202102
[43] Lv H *et al* 2009 *Appl. Phys. Lett.* **94** 213502